Biosensors and Bioelectronics 142 (2019) 111523

Contents lists available at ScienceDirect

Biosensors and Bioelectronics

journal homepage: www.elsevier.com/locate/bios

Absolute quantification and analysis of extracellular vesicle lncRNAs from the peripheral blood of patients with lung cancer based on multi-colour fluorescence chip-based digital PCR

Yanan Bai[a,b,1], Youlan Qu[a,c,1], Zhenhua Wu[a], Yijiu Ren[d], Zule Cheng[a,b], Yunxing Lu[a,b], Jie Hu[e], Jiatao Lou[f], Jianlong Zhao[a], Chang Chen[d,**], Hongju Mao[a,b,*]

[a] State Key Laboratory of Transducer Technology, Shanghai Institute of Microsystem and Information Technology, Chinese Academy of Sciences, Shanghai, 200050, China
[b] Center of Materials Science and Optoelectronics Engineering, University of Chinese Academy of Sciences, Beijing, 100049, China
[c] School of Stomatology, Dalian Medical University, Dalian, 116044, China
[d] Department of Thoracic Surgery, Shanghai Pulmonary Hospital, Tongji University School of Medicine, Shanghai, 200443, China
[e] Department of Pulmonary Medicine, Zhongshan Hospital, Fudan University, Shanghai, 200032, China
[f] Department of Laboratory Medicine, Shanghai Chest Hospital, Shanghai Jiaotong University, Shanghai, 200030, China

ARTICLE INFO

Keywords:
Lung cancer
Extracellular vesicles
lncRNA
Early diagnosis
Multi-colour fluorescence

ABSTRACT

Emerging evidence indicates that extracellular vesicle (EV) long non-coding ribonucleic acids (lncRNAs) in lung cancer may be clinically useful biomarkers for early diagnosis using liquid biopsy. However, the extremely low quantities of EV-lncRNAs in peripheral blood are a major challenge for multi-target detection. In this study, we developed a new multi-colour fluorescence digital PCR EV-lncRNA (miDER) analysis chip, and then demonstrated its ability to quickly and accurately analyse the levels of two target genes and one reference gene from peripheral blood. Under the miDER assay, the limit of detection of the target gene from peripheral blood was 10 copies/μL. Based on multiplex assay, the expression levels of two lung cancer-related genes (*SLC9A3-AS1* and *PCAT6*) in patients with lung cancer (n = 32) and healthy controls (n = 30) showed a significant difference between the two groups ($P < 0.001$; two-tailed *t*-test). A receiver operating characteristic (ROC) curve analysis was used to evaluate the discrimination ability of these lncRNAs. The combination of two lncRNAs in the miDER assay yielded a higher area under curve (AUC) value of 0.811 (95% CI = 0.705–0.918). Moreover, to determine the absolute quantitation capacity of the miDER assay, we compared the results to those obtained by quantitative real-time polymerase chain reaction (qPCR), demonstrating that the miDER assay is more sensitive than qPCR. The multiplex assay based on the miDER could provide a new solution for the multi-index combined detection of trace EV-lncRNAs in body fluids and demonstrate the use of EV-lncRNAs as biomarkers for lung tumour biopsy.

1. Introduction

Lung cancer is the most common malignant tumour with the highest incidence worldwide, accounting for the largest number of cancer deaths. Due to the complexity of lung tissues, the absence of obvious symptoms in the early stage, and the easy spread and metastasis, lung cancer is typically diagnosed at an intermediate or advanced stage. The early detection of lung cancer is mainly based on imaging and tumour protein markers (Hirsch et al., 2001; Wulfkuhle et al., 2003). Advanced imaging techniques, such as multi-slice spiral computed tomography (CT) and positron emission tomography can detect tumours with a diameter of about 2–6 mm. Low-dose spiral CT has high sensitivity and avoids other traumatic examinations. However, owing to its high sensitivity, the false positive rate is high, leading to over-diagnosis, false alarms, and unnecessary examinations, biopsies, and operations (Stanley, 2001; Swensen et al., 2003). Therefore, the identification of true positives and false positives after screening by low-dose CT is an urgent issue.

Lung tissue biopsy can provide high diagnostic accuracy. However, this approach is inconvenient and invasive and may lead to additional

* Corresponding author. State Key Laboratory of Transducer Technology, Shanghai Institute of Microsystem and Information Technology, Chinese Academy of Sciences, Shanghai, 200050, China.
** Corresponding author. Department of Thoracic Surgery, Shanghai Pulmonary Hospital, Tongji University School of Medicine, Shanghai, 200443, China.
E-mail addresses: changchenc@hotmail.com (C. Chen), hjmao@mail.sim.ac.cn (H. Mao).
[1] Yanan Bai and Youlan Qu contribute to this work equally.

https://doi.org/10.1016/j.bios.2019.111523
Received 17 May 2019; Received in revised form 3 July 2019; Accepted 16 July 2019
Available online 17 July 2019
0956-5663/

complications (Bensard et al., 1993; Yung, 2003). There is thus a critical need for non-invasive and highly sensitive diagnostic methods to improve early diagnosis and outcomes. Bodily fluids, such as blood, are considered ideal samples for disease diagnosis (Goessl et al., 2001; Johnson and Lo, 2002). Prior research has shown that extracellular vesicles (EVs), including exosomes and microvesicles, can be readily harvested from the blood for further analysis and thus represent an attractive source of tumour-derived materials (Yanez-Mo et al., 2015).

EVs are specialized membranous, nanosized endocytic vesicles that are secreted by most cells (Colombo et al., 2014). In particular, EVs secreted from tumour cells are closely related to tumour development, immune escape, and the tumour microenvironment (Kalluri, 2016). They are abundant, stable, and contain unique proteins and nucleic acids (e.g. DNAs, mRNAs, miRNAs, and lncRNAs) reflective of their cells of origin (Mateescu et al., 2017; Thakur et al., 2014). Emerging evidence indicates that long non-coding ribonucleic acids (lncRNAs) from the peripheral blood are potential cancer biomarkers. LncRNAs are defined as transcripts with a minimum length of 200 nucleotides and limited protein-coding potential; deregulated expression can not only differentiate normal populations and patients with lung cancer but is also associated with the occurrence and development of lung cancer (Mercer et al., 2009; Ponting et al., 2009). In our previous study, we screened differentially expressed lncRNAs in early lung cancer tissues and demonstrated that they may be clinically useful biomarkers for early diagnosis (Cheng et al., 2017; Wang et al., 2015). However, owing to the difficulty in obtaining tissue samples from patients suspected to have lung cancer, the development of a sensitive, accurate, and cost-effective method using circulating, EV-lncRNAs as biomarkers is needed for diagnosis.

Existing lncRNA detection methods include quantitative real-time polymerase chain reaction (qPCR) (Schmittgen et al., 2008; Shi and Chiang, 2005), microarray (Akama et al., 2009; Liu et al., 2008), next-generation sequencing (Chen et al., 2009), and surface-enhanced Raman spectroscopy (SERS) (Driskell et al., 2008). SERS-based methods are limited by a lack of spectral reproducibility of the SERS substrate for early detection. Next-generation sequencing-based molecule counting relies on complex library preparation schemes, and high sequencing depths are required to achieve high sensitivity. Using microarray and qPCR methods, it is difficult to detect targets with low copy numbers. It has been reported that the content of lncRNAs in EVs is very low; far lower than their mRNA level (Li et al., 2019). Therefore, there is a need for a more sensitive, accurate, and convenient quantitative method to study low-abundance EV-lncRNA.

Digital polymerase chain reaction (dPCR) (Sykes et al., 1992; Vogelstein and Kinzler, 1999) is a single molecule detection technology. This end point method does not require standard curves, shows high precision for the quantification of low-abundance EV-lncRNA targets, and is resistant to residual PCR inhibitors. However, existing dPCR systems involve several sophisticated instruments for droplet generation, PCR cycling, and read-out (Vogelstein and Kinzler, 1999). Moreover, the sensitivity and multiplexing capability of commercial droplet PCR systems are limited by the total number of droplets that can be generated and analysed per run (Huggett et al., 2015; Zhong et al., 2011). Consequently, multiple sophisticated instrumentation, prolonged image acquisition, low detection throughput, and high cost limit their broad implementation.

To address these limitations, in this study, we developed a simple, sensitive, accurate, high-throughput, and low-cost microfluidic platform termed multi-colour fluorescence digital PCR EV-lncRNA (miDER) analysis, which enables a fast, on-chip analysis of EV-lncRNA expression. The sensitivity and specificity for tumour diagnosis using a single marker are limited, while the combined detection of multiple markers usually has higher sensitivity and specificity, which can further improve the accuracy of tumour diagnosis. The miDER system uses multiplex PCR technology combined with a microfluidic chip to partition and amplify the sequences, which can simultaneously detect multi-target EV-lncRNAs present at very low levels, improve detection throughput, and reduce sample and reagent dosages. We explored the feasibility of multiplex fluorescent dPCR and determined the lower limit of detection of the chip. Using the newly developed technology, we identified two key EV-lncRNA markers in our pre-screened lncRNAs from early lung cancer tissues (Cheng et al., 2017; Wang et al., 2015) and compared the results obtained using our chip and qPCR to prove that our miDER system has higher sensitivity than that of qPCR. Furthermore, we analysed clinical blood samples from patients with confirmed lung cancer and showed that EV-lncRNA expression was associated with lung tumours, supporting the use of EV-lncRNA as biomarkers for lung tumour biopsy.

2. Material and methods

2.1. Sample preparation

Samples were obtained from 32 patients who had not undergone primary surgical resection of lung cancer and 30 healthy controls in 2017 at Shanghai Zhongshan Hospital. Healthy controls were recruited from people who underwent a routine health check-up and showed no disease. Demographic and clinical characteristics of subjects are summarized in Tables S–1. All subjects gave informed consent prior to sample collection. The pathological stage of each sample was determined by an experienced pathologist according to the TNM (Tumour-Node-Metastasis) classification of malignant tumours. All aspects of this study were approved by the Institutional Review Board of Shanghai Zhongshan Hospital, China. Medical records, including sex, age, tumour location, differentiation, tumour size, and local invasion, were obtained. Patients with lung cancer with incomplete medical records, prior chemotherapy or radiation, lost to follow-up, or withdrawal of consent were excluded from this study.

Peripheral blood samples were collected by venipuncture from all subjects. Cell-free plasma was isolated using a two-step centrifugation protocol, $1900 \times g$ for 10 min and $3000 \times g$ for 15 min at 4 °C, followed by EVs extraction or storage at −80 °C. Blood samples with hemolysis were excluded. EVs from 1.5 mL of prefiltered plasma were isolated using a procedure modified from the exoRNeasy protocol described in the exoRNeasy Serum/Plasma Handbook, and the isolated EVs were characterized and analysed as shown in Figure S-1. EV-RNA was extracted from plasma using the exoRNeasy Serum/Plasma Midi Kit (QIAGEN, Hilden, Germany) according to the manufacturer's instructions and evaluated using a NanoDrop spectrophotometer (Thermo Fisher Scientific, Waltham, MA, USA). Extracted exoRNA (100 ng) was reverse-transcribed to first-strand complementary DNA (cDNA) using a SuperScript III First-Strand Synthesis System (Invitrogen, Carlsbad, CA, USA). Then, the cDNA samples were stored at 4 °C until subsequent dPCR amplification.

2.2. Gene selection, primers, and probes

The expression levels of two lung cancer-related genes (*SLC9A3-AS1* and *PCAT6*) identified in our previous studies (Cheng et al., 2017; Wang et al., 2015) were evaluated in EVs samples. *GAPDH* was used as a reference gene. Primers and TaqMan probes for three RNAs were designed using Primer Premier 6.0. They were synthesized and purified by high-performance liquid chromatography by Sangon Biotech (Shanghai, China), resuspended separately at 100 μM in deionized water, and stored at −20 °C. Sequences of the primers and TaqMan probes are listed in Tables S–2.

2.3. Design and fabrication of the miDER chip

As shown in Fig. 1, a self-partitioning microfluidic chip containing 21,760 independent microchambers was used. To fabricate the chip, a photoresist (SU-8 3050) was spin-coated onto a 4″ silicon wafer to

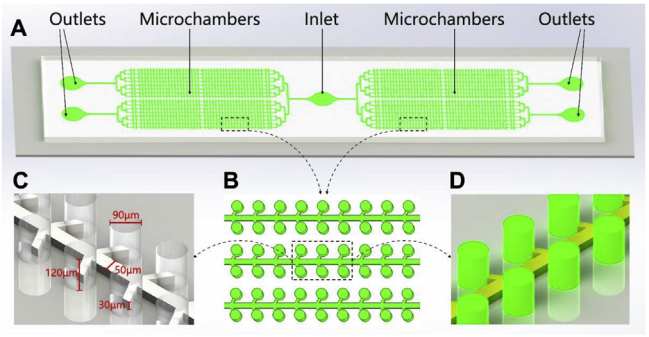

Fig. 1. Layout of the microfluidic chip. (A) Thumbnail of the chip structure. (B) Schematic diagram of microchambers arrangement. (C) Size of the microchamber and the channel. (D) Schematic diagram of the microchambers after injection.

create approximately 30-μm (3500 rpm for 40 s) channels. After the wafer was soft-baked (95 °C for 15 min), the channels were patterned by ultraviolet (UV) exposure with a photolithography mask. Then, the wafer was put onto a hotplate for a post-exposure bake (PEB) (94 °C for 5 min). After the completion of the first layer (flow channel), a second photoresist layer (microchambers) (SU-8 3050) was spin-coated to a thickness of 120 μm (1000 rpm for 40 s) on the wafer. The second layer was used to fabricate the microchambers. After the second exposure, PEB, and development of the wafer, the microchamber mould was also patterned on the wafer. Finally, the mould was baked (180 °C for 45 min) on a hotplate to harden it for repeated use (Figure S-2). The width and height of the channels were 50 and 30 μm, respectively. The diameter of the cylindrical microchamber was 90 μm, with a height of 120 μm. Based on these dimensions, the volume of the microchamber was approximately 0.76 nL.

After the preparation of the mould, a 10:1:0.05 (w/w/w) mixture of Sylgard 184 resin (Polydimethylsiloxane, PDMS), cross-linker, and Triton X-100 (Sigma-Aldrich, St. Louis, MO, USA) was degassed under a vacuum and poured into the mould to form a 2-mm-thick structured microfluidic substrate. Triton X-100 was added to prevent reaction components from being adsorbed during the reaction (Fu et al., 2017). After baking the mould (70 °C for 50 min), PDMS was gently peeled off and cut to the appropriate size. Finally, the structured microfluidic substrate was bonded to a glass microscope slide (1 mm) by thermal bonding (85 °C for 10 min) after pre-coating with a thin layer of PDMS (Figure S-3).

2.4. Quantitative real-time PCR

QPCR was performed using a standard TaqMan PCR kit protocol on a LightCycler 480 II (Roche, Basel, Switzerland). The 20-μL PCR volume included 2 μL of cDNA, 1.5 μL of primer and probe mix, 10 μL of Probes Master (Roche), and 6.5 μL of deionized water. The reactions were incubated in a 96-well plate at 95 °C for 10 min, followed by 40 cycles of 95 °C for 15 s and 60 °C for 45 s. All qPCRs were performed in triplicate and relative quantification was performed for each sample by normalizing with respect to *GAPDH* expression. No signal amplification was observed when water was added instead of the sample.

2.5. Quantification and analysis using the miDER chip

To validate the lncRNA expression levels of selected genes, the cDNA samples (synthesized from lncRNA) were quantitated using a miDER chip. The 20-μL reaction mixture contained 2 μL of the cDNA sample, 2 × LightCycler 480 Probes Master (Roche), 250 nM each primer, 250 nM TaqMan probe, 0.3% Triton X-100 (v/v), and deionized water (Sangon Biotech). Before use, the chip was degassed in a vacuum system (10 kPa) for 60 min. When in use, the reaction mixture was dropped onto the inlet of the chip (Fig. 1). The pressure difference of the air dissolved in PDMS (Hosokawa et al., 2004) would provide inner power to suck the reaction mixture into the channels and microchambers. When the reaction mixture was completely drawn into the microchambers, the oil phase (silicone oil, Sylgard 184 resin, and cross-linker, 4:1:0.1 (w/w/w)) was added to the inlet. The oil phase drained the reaction mixture from the channel, so that all microchambers were isolated individually. Finally, a cover glass was attached to the surface of the chip to complete the package (Figure S-4). Thermocycling was performed using an Eppendorf Mastercycler® nexus flat. The amplification process included the activation of FastStart Taq DNA polymerase at 95 °C for 10 min, followed by 40 cycles of amplification (95 °C for 15 s and 60 °C for 45 s), and preservation at 10 °C. The miDER chip was observed using a fluorescence microscope (BX51; OLYMPUS, Tokyo, Japan) equipped with a 100 W mercury lamp, a 4 × objective lens, a charge-coupled device (CCD) camera (Olympus DP70), and filters. Two-dimensional (2D) fluorescence bitmap images were captured using the CCD camera, and the positive reactions in the microchambers were counted. The number of target cDNA templates was calculated by Poisson statistics: $\lambda = -\ln(1-p)$, where p is the fraction of positive reactions and λ represents target copies per microchamber. Thus, copy numbers of target cDNA molecules were easily obtained (Quan et al., 2013; Zhong et al., 2011). Finally, the lncRNA expression level was calculated by the following equation: expression level = Copy number of target gene / Copy number of reference gene.

3. Results and discussion

3.1. Principle of multi-colour fluorescence dPCR EV-lncRNA detection

As shown in Fig. 2A, our technique comprises four key steps, i.e. sample preparation, mixture partitioning, amplification, and quantification. In the first step, cDNA (synthesized from lncRNA), DNA polymerases, primers, TaqMan probes, dNTPs, and buffer solution (Mg^{2+}) were mixed into a PCR mixture. In the second step, the reaction mixture was partitioned by the miDER chip into many independent microchambers, some of which contained the target cDNA, while others did not. In the third step, the PCR amplification process was performed on the miDER chip, consisting of two distinct temperature stages. During amplification, the reactions containing the target sequence were amplified by a million-fold or more and the signals accumulated. However, there was no signal accumulation without target sequence reactions. Finally, 2D fluorescence bitmap images were acquired using a CCD camera and analysed separately to detect the presence (positive reactions) or absence (negative reactions) of an endpoint signal. Considering that multiple target molecules may be present in a single microchamber, Poisson model correction was used to determine the copy number of the target cDNAs, and the lncRNA expression level was calculated. Multi-target detection was completed by a single amplification, and different target cDNAs produced different fluorescence signals during PCR amplification (schematic diagram shown in Fig. 2B).

We used the microfluidic chip for multi-colour fluorescence dPCR EV-lncRNA analyses. For the simultaneous detection of multiple targets, we initially tested four fluorophores, FAM (excitation: 485, emission: 524), HEX (excitation: 534, emission: 572), ROX (excitation: 550, emission: 630), and CY5 (excitation: 649, emission: 670) with different excitation and emission wavelengths for dPCR amplification. In subsequent experiments, however, we detected interference between the fluorophores HEX and ROX, which was verified in our later PCR experiments (Figure S-5). Finally, we selected three fluorophores, FAM, HEX, and CY5, for the single detection of three different EV-RNA targets using our miDER assay (Fig. 2C).

3.2. Determination of the copy number detection limit by miDER chip

To test the sensitivity of our chip for EV-lncRNA detection, cDNA

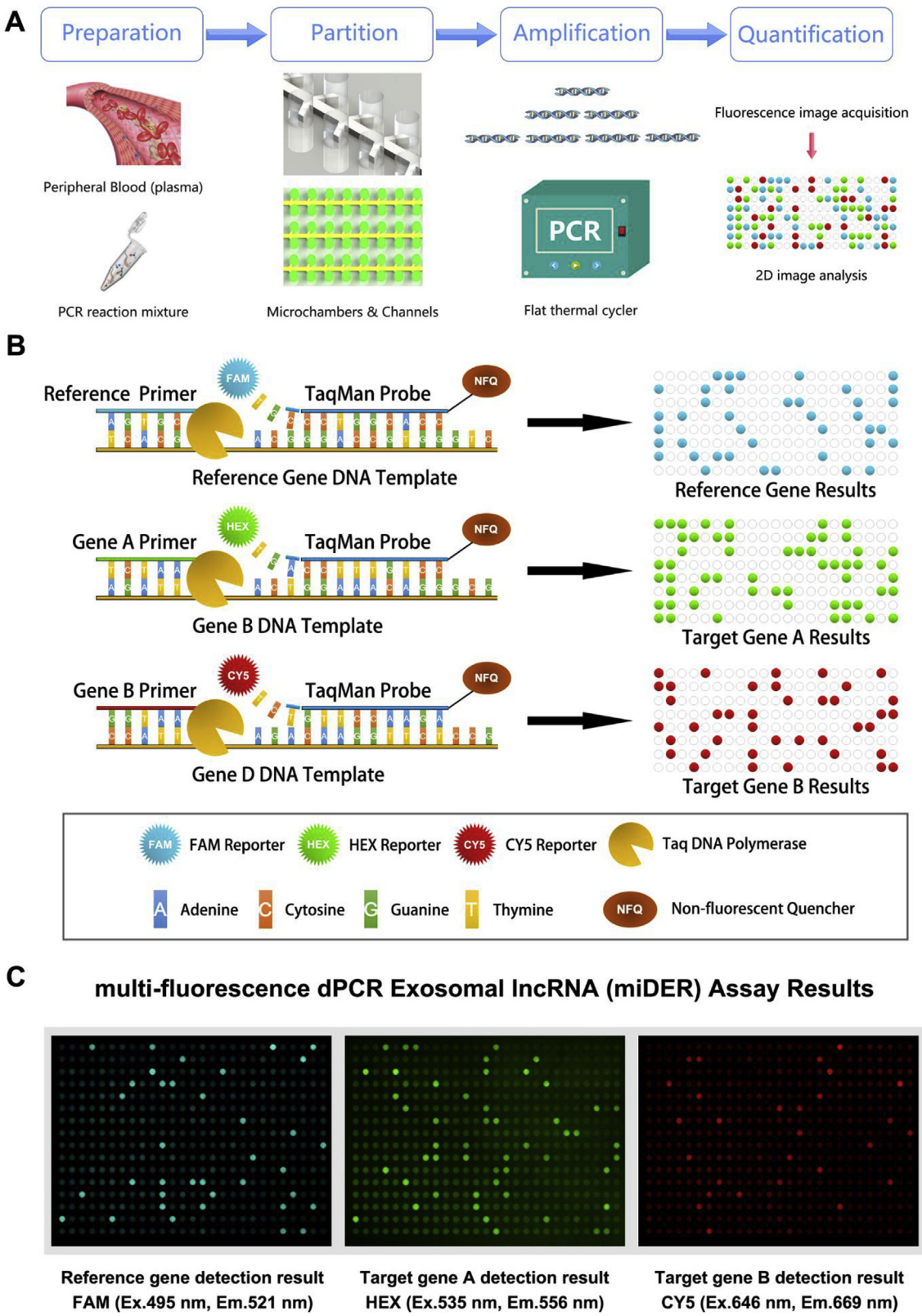

Fig. 2. Principle of digital PCR-based multiple detection. (A) Four key steps: sample preparation, mixture partitioning, amplification process, and quantification process. (B) Schematic representation of the hydrolysis of different TaqMan probes followed by the generation of different positive fluorescence signals. (C) Fluorescence signals in the miDER assay were obtained using three fluorescence excitation channels, with light excitation at 485 nm (FAM), 534 nm (HEX), and 649 nm (CY5) for *GAPDH* (Reference Gene), *SLC9A3-AS1* (Target Gene A), and *PCAT6* (Target Gene B), respectively.

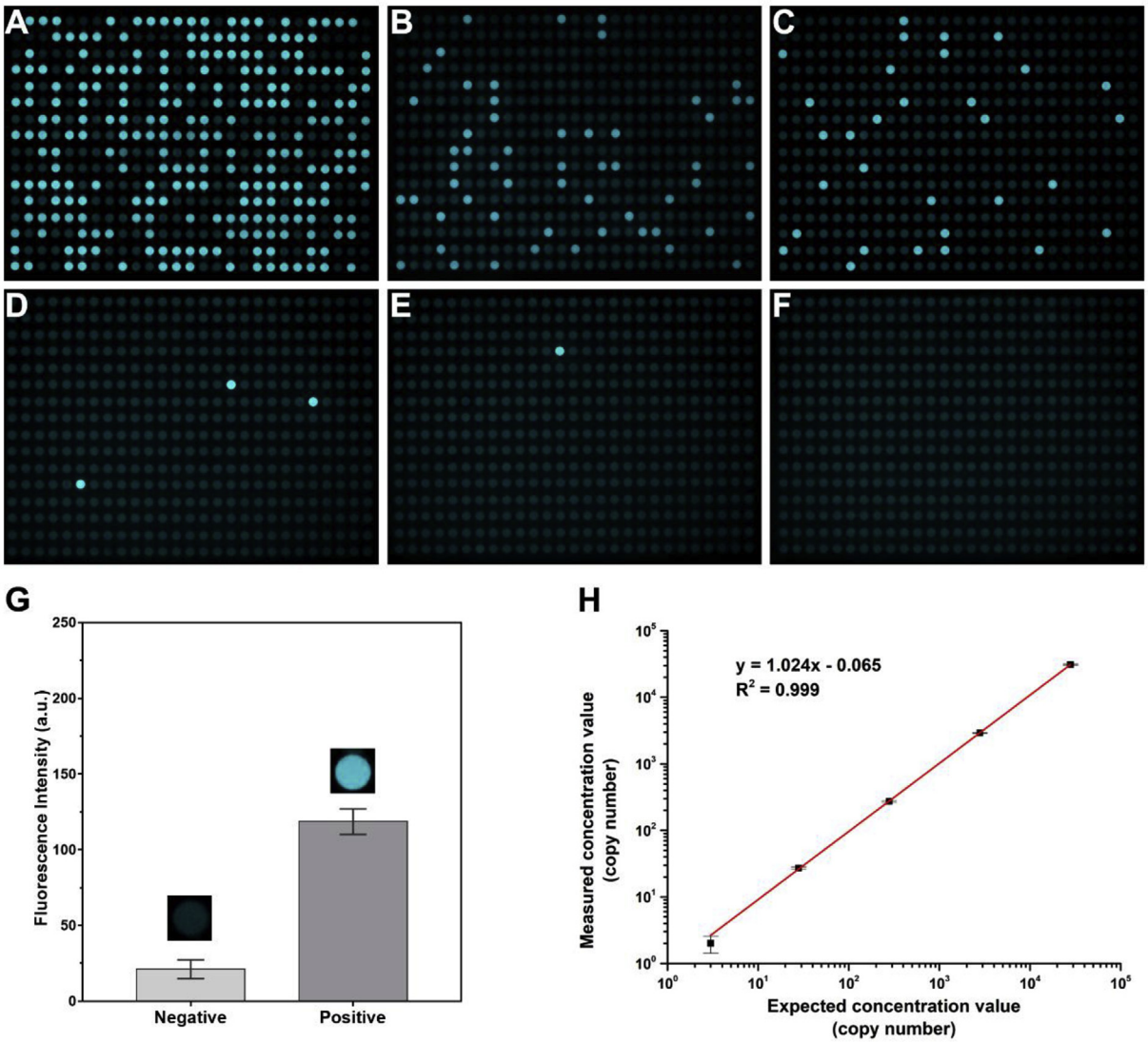

Fig. 3. Determination of the copy number detection limit for the miDER chip. Concentrations of templates (*GAPDH*) were (A) 2.9×10^4copies/μL, (B) 10^4 copies/μL, (C) 10^3 copies/μL, (D) 10^2 copies/μL, and (E) 10 copies/μL. (F) No cDNA template was loaded in the control sample, and no positive microchamber was observed. (G) 2D fluorescence bitmap images were acquired using a CCD camera, and the fluorescence intensity of the positive (right) or negative (left) endpoint signal was analysed using Image-Pro Plus (Media Cybernetics, Rockville, MD, USA). The fluorescence intensity of the positive reaction was significantly higher than that of the negative reaction. Error bars represent the standard deviation based on the entire chip's microchambers (21,760). (H) The experimentally measured concentrations were highly consistent with the expected concentrations (R^2 = 0.999). All experiments were performed in triplicate and the data are shown as means ± s.d.

templates ranging from 2.9×10^4 copies/μL to 10^1 copies/μL were prepared. The reaction mixture was dispersed by the miDER chip into many independent microchambers, a portion of which contained the target cDNA. The results for different concentrations of cDNA templates after PCR amplification are shown in Fig. 3A–E. Three blank samples were tested and none of them yielded a positive reaction (Fig. 3F). In this study, since the cDNA template was partitioned into isolated microchambers for amplification, only two kinds of endpoint signals (positive or negative) were produced. Therefore, the number of target templates in a sample is determined by the number of "positive" microchambers on the chip. Then, the copy number of target cDNA was determined by Poisson statistics. As shown in Fig. 3G, the average fluorescence intensity of the positive microchambers was significantly higher than that of the negative microchambers ($P < 0.0001$; two-tailed *t*-test). Using *k*-means clustering, it is convenient to distinguish between the positive and negative microchambers. As the concentration of templates decreased, the number of positive reactions also decreased (R^2 = 0.999), as shown in Fig. 3H. These results indicate that the detection limit of the chip was 10 copies/μL.

3.3. Quantitative detection of the lncRNA copy number by the miDER chip and comparison with qPCR results and commercial QX200™ dPCR system results

The aim of this study was to quantify EV-lncRNA expression; accordingly, the detection equipment needs to have an accurate quantitative capacity. To determine the absolute quantitation capacity of our chip, we compared the results to those obtained by qPCR. A series of cDNA samples (from 10^5 to 10^1) was prepared and quantified using our chip and qPCR (LightCycler 480 II; Roche). The quantitative results obtained using the chip are shown in Fig. 4A. When the cDNA sample concentration decreased, the positive reactions also decreased, and a copy number of 10^1 could be quantified. The quantitative results obtained by qPCR are shown in Fig. 4B. When the copy number of the cDNA sample was below 10^2, the qPCR results were negative (Fig. 4B, yellow lines, Cp > 35). When we tried to extend the qPCR cycles to 45, a copy number of 10^1 could still not get the available Cp value. For copy numbers of between 10^5 and 10^2, there was a linear relationship between our chip results and the qPCR results (R^2 = 0.999), as shown in

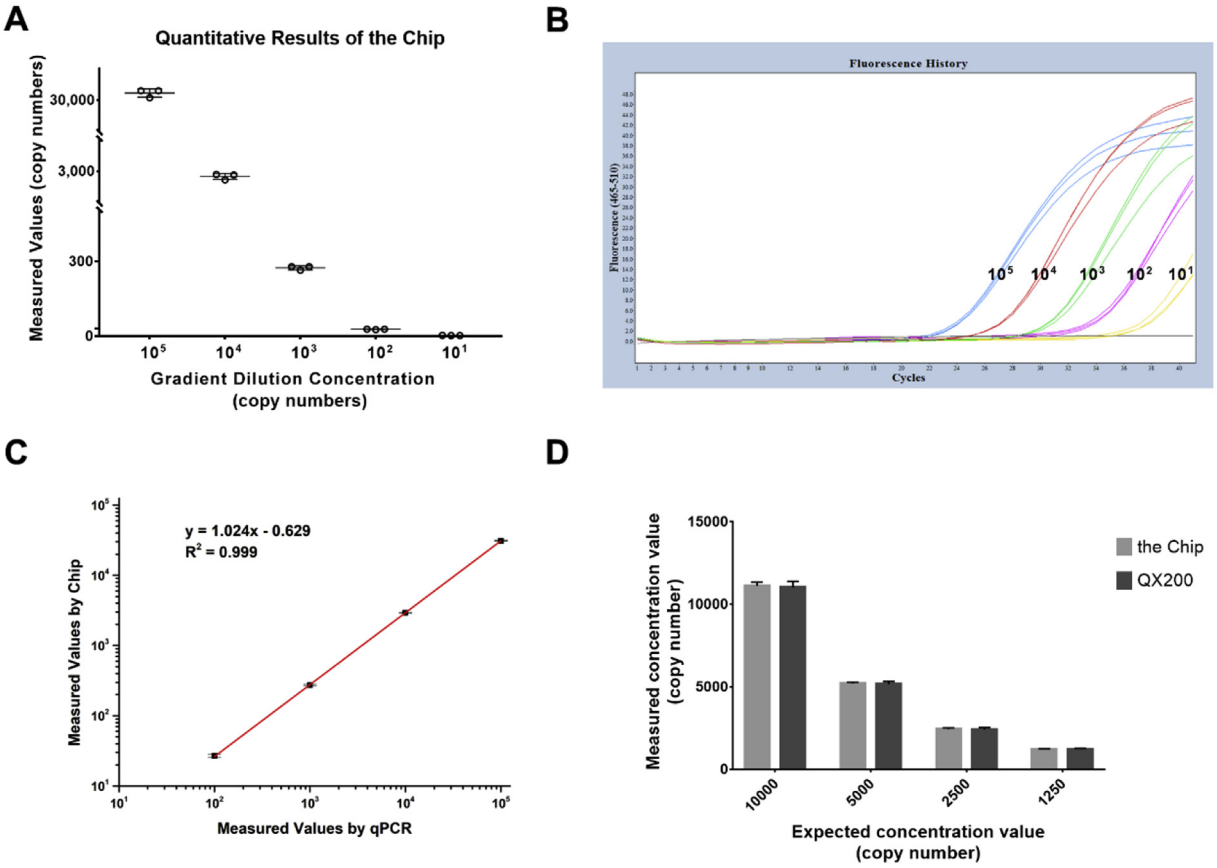

Fig. 4. Quantitative detection of the lncRNA copy number using the miDER chip, qPCR and commercial droplet dPCR system. (A) Quantitative results obtained using the miDER chip. (B) Quantitative results obtained by qPCR. The qPCR results were negative when the cDNA sample concentration was below 10^2 (yellow lines, Cp > 35). (C) There was a linear relationship between our chip results and the qPCR results (R^2 = 0.999). (D) Quantitative results by the miDER chip and comparison with QX200™ Droplet Digital PCR System results. All experiments were performed in triplicate and the data are shown as means ± s.d. (For interpretation of the references to colour in this figure legend, the reader is referred to the Web version of this article.)

Fig. 4C. In addition, a series of cDNA samples with half-gradient dilution was prepared and quantified using our chip and commercial dPCR system (QX200 ™; Bio-Rad). Fig. 4D shows that the results were highly consistent. This indicates that the absolute quantitative capability of our miDER chip is comparable to that of the commercial dPCR system. In addition, droplet digital PCR has the problem of droplet burst or fusion. And the droplet digital system demands higher operational requirements, resulting in a large fluctuation in the number of droplets. While the lower number of droplets will seriously affect the accuracy of absolute quantification of digital PCR. Compared to the droplet digital PCR platform, our chip has the following advantages: (i) The cost of our miDER chip is much lower than that of the commercial dPCR system; (ii) Only one fluorescence microscope and one general in-situ PCR instrument were needed in the method, while QX200™ requires up to four special devices; (iii) Our miDER chip could detect more targets than QX200™ in a single reaction. Therefore, these results demonstrate that our miDER chip can be used to quantify the expression of EV-lncRNAs.

3.4. Analysis of clinical samples

To test the utility of the miDER assay in lung biopsy, we conducted a clinical feasibility study. Gene product levels in EVs from clinical peripheral blood samples exhibited heterogeneity. Although we tried to maintain a consistent starting volume of clinical peripheral blood samples, there were still substantial fluctuations in the target gene levels of healthy controls. Therefore, we used the reference gene *GAPDH* for normalization. The average levels of *SLC9A3-AS1* and *PCAT6* were significantly higher (P = 0.0008 and P = 0.0069; two-tailed t-test) in lung cancer samples (n = 32) than in healthy controls (n = 30) (Fig. 5A–B). A receiver operating characteristic (ROC) curve analysis was used to evaluate the discrimination ability of these lncRNAs. Using a single marker, EV *SLC9A3-AS1* and *PCAT6* yielded area under curve (AUC) values of 0.760 (95% CI = 0.643–0.878) and 0.705 (95% CI = 0.575–0.835), respectively, for identifying patients with lung cancers (Fig. 5C). The combination of these lncRNAs in the miDER assay yielded a higher AUC value of 0.811 (95% CI = 0.705–0.918) (Fig. 5D).

4. Conclusion

We developed a new chip, miDER, which enables high-sensitivity, multi-target (*GAPDH, SLC9A3-AS1*, *PCAT6*) detection in a single PCR amplification of a single microfluidic chip. The newly developed technology has many advantages, including its simplicity, high sensitivity, and low cost. It can effectively detect EV-lncRNA in clinical blood samples. With the miDER, we demonstrated (i) the feasibility of the EV-lncRNA multiplex fluorescent digital PCR microfluidic chip, (ii) the reliable detection of EV-lncRNAs in patient blood, and (iii) the ability to effectively distinguish lung cancer cases from healthy controls by detecting the EV-lncRNA expression levels of *SLC9A3-AS1* and *PCAT6*. In addition, detection could be extended to other tumour types by identifying target genes. Large data sets are needed to validate the clinical utility of miDER. Although we originally developed the miDER technology for early diagnosis, it could be adapted for tumour prognosis and recurrence monitoring, e.g. the long-term directional monitoring of EV-lncRNA. If used in conjunction with chest X-ray, CT, and other ancillary

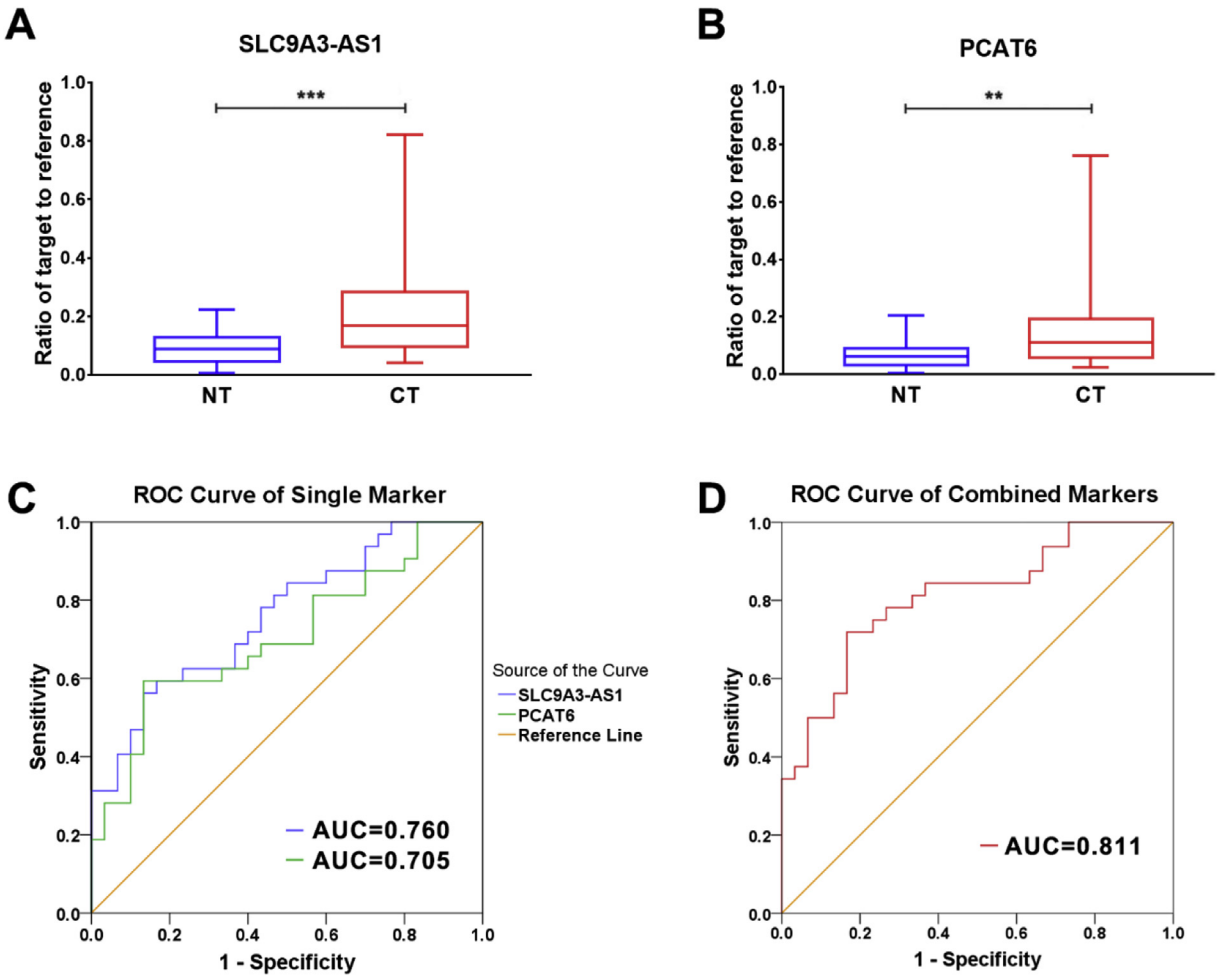

Fig. 5. Quantitative analyses of EV-lncRNAs in clinical samples and ROC curve analysis. (A–B) The expression level of two lncRNAs in 32 lung cancer samples (CT) and 30 healthy controls (NT). All differences in lncRNAs between CT and NT were significant. ROC curves for the detection of lung cancer using EV *SLC9A3-AS1* (C blue line), *PCAT6* (C green line), and their combination by miDER assays (D), as assessed by AUC. AUC: area under the curve. **P < 0.01 (two-tailed *t*-test); ***P < 0.001 (two-tailed *t*-test). (For interpretation of the references to colour in this figure legend, the reader is referred to the Web version of this article.)

tests, the EV-lncRNA test could obviate or reduce the need for biopsy in a population of patients with lung cancer. We propose that if validated using a larger cohort, our multi-colour fluorescence digital PCR chip approach can provide a new solution for the combined detection of trace EV-lncRNAs in body fluids, thereby providing a new strategy for the early diagnosis and treatment of lung cancer.

Declaration of competing interest

The authors declare that they have no known competing financial interests or personal relationships that could have appeared to influence the work reported in this paper.

CRediT authorship contribution statement

Yanan Bai: Conceptualization, Methodology, Formal analysis, Investigation, Writing - original draft. **Youlan Qu:** Conceptualization, Methodology, Validation, Writing - original draft. **Zhenhua Wu:** Methodology, Visualization. **Yijiu Ren:** Resources. **Zule Cheng:** Formal analysis. **Yunxing Lu:** Data curation. **Jie Hu:** Resources. **Jiatao Lou:** Resources. **Jianlong Zhao:** Supervision. **Chang Chen:** Resources, Supervision. **Hongju Mao:** Conceptualization, Writing - review & editing, Supervision, Project administration, Funding acquisition.

Acknowledgment

This study was supported by Grants from National Key Research and Development Program, China (No. 2018YFA0108202 and 2017YFA0205300), National Science Foundation, China (No. 61571429, 61571077,61801464 and 61801465) and the Science and Technology Commission of Shanghai Municipality, China (No. 16410711800 and 17JC1401001).

Appendix A. Supplementary data

Supplementary data to this article can be found online at https://doi.org/10.1016/j.bios.2019.111523.

References

Akama, T., Suzuki, K., Tanigawa, K., Kawashima, A., Wu, H., Nakata, N., Osana, Y., Sakakibara, Y., Ishii, N., 2009. Whole-genome tiling array analysis of Mycobacterium leprae RNA reveals high expression of pseudogenes and noncoding regions. J. Bacteriol. 191 (10), 3321–3327.

Bensard, D.D., McIntyre Jr., R.C., Waring, B.J., Simon, J.S., 1993. Comparison of video thoracoscopic lung biopsy to open lung biopsy in the diagnosis of interstitial lung disease. Chest 103 (3), 765–770.

Chen, X., Li, Q., Wang, J., Guo, X., Jiang, X., Ren, Z., Weng, C., Sun, G., Wang, X., Liu, Y., Ma, L., Chen, J.Y., Wang, J., Zen, K., Zhang, J., Zhang, C.Y., 2009. Identification and characterization of novel amphioxus microRNAs by Solexa sequencing. Genome Biol. 10 (7), R78.

Cheng, Z., Bai, Y., Wang, P., Wu, Z., Zhou, L., Zhong, M., Jin, Q., Zhao, J., Mao, H., Mao,

H., 2017. Identification of long noncoding RNAs for the detection of early stage lung squamous cell carcinoma by microarray analysis. Oncotarget 8 (8), 13329–13337.
Colombo, M., Raposo, G., Thery, C., 2014. Biogenesis, secretion, and intercellular interactions of exosomes and other extracellular vesicles. Annu. Rev. Cell Dev. Biol. 30, 255–289.
Driskell, J.D., Seto, A.G., Jones, L.P., Jokela, S., Dluhy, R.A., Zhao, Y.P., Tripp, R.A., 2008. Rapid microRNA (miRNA) detection and classification via surface-enhanced Raman spectroscopy (SERS). Biosens. Bioelectron. 24 (4), 923–928.
Fu, Y.Y., Zhou, H.B., Jia, C.P., Jing, F.X., Jin, Q.H., Zhao, J.L., Li, G., 2017. A microfluidic chip based on surfactant-doped polydimethylsiloxane (PDMS) in a sandwich configuration for low-cost and robust digital PCR. Sens. Actuators B Chem. 245, 414–422.
Goessl, C., Muller, M., Heicappell, R., Krause, H., Miller, K., 2001. DNA-based detection of prostate cancer in blood, urine, and ejaculates. Ann. N. Y. Acad. Sci. 945, 51–58.
Hirsch, F.R., Franklin, W.A., Gazdar, A.F., Bunn Jr., P.A., 2001. Early detection of lung cancer: clinical perspectives of recent advances in biology and radiology. Clin. Cancer Res. 7 (1), 5–22.
Hosokawa, K., Sato, K., Ichikawa, N., Maeda, M., 2004. Power-free poly(dimethylsiloxane) microfluidic devices for gold nanoparticle-based DNA analysis. Lab Chip 4 (3), 181–185.
Huggett, J.F., Cowen, S., Foy, C.A., 2015. Considerations for digital PCR as an accurate molecular diagnostic tool. Clin. Chem. 61 (1), 79–88.
Johnson, P.J., Lo, Y.M., 2002. Plasma nucleic acids in the diagnosis and management of malignant disease. Clin. Chem. 48 (8), 1186–1193.
Kalluri, R., 2016. The biology and function of exosomes in cancer. J. Clin. Investig. 126 (4), 1208–1215.
Li, Y., Zhao, J., Yu, S., Wang, Z., He, X., Su, Y., Guo, T., Sheng, H., Chen, J., Zheng, Q., Li, Y., Guo, W., Cai, X., Shi, G., Wu, J., Wang, L., Wang, P., He, X., Huang, S., 2019. Extracellular vesicles long RNA sequencing reveals abundant mRNA, circRNA, and lncRNA in human blood as potential biomarkers for cancer diagnosis. Clin. Chem. 65 (6), 798–808.
Liu, C.G., Spizzo, R., Calin, G.A., Croce, C.M., 2008. Expression profiling of microRNA using oligo DNA arrays. Methods 44 (1), 22–30.
Mateescu, B., Kowal, E.J., van Balkom, B.W., Bartel, S., Bhattacharyya, S.N., Buzas, E.I., Buck, A.H., de Candia, P., Chow, F.W., Das, S., Driedonks, T.A., Fernandez-Messina, L., Haderk, F., Hill, A.F., Jones, J.C., Van Keuren-Jensen, K.R., Lai, C.P., Lasser, C., Liegro, I.D., Lunavat, T.R., Lorenowicz, M.J., Maas, S.L., Mager, I., Mittelbrunn, M., Momma, S., Mukherjee, K., Nawaz, M., Pegtel, D.M., Pfaffl, M.W., Schiffelers, R.M., Tahara, H., Thery, C., Tosar, J.P., Wauben, M.H., Witwer, K.W., Nolte-'t Hoen, E.N., 2017. Obstacles and opportunities in the functional analysis of extracellular vesicle RNA - an ISEV position paper. J. Extracell. Vesicles 6 (1), 1286095.
Mercer, T.R., Dinger, M.E., Mattick, J.S., 2009. Long non-coding RNAs: insights into functions. Nat. Rev. Genet. 10 (3), 155–159.
Ponting, C.P., Oliver, P.L., Reik, W., 2009. Evolution and functions of long noncoding RNAs. Cell 136 (4), 629–641.
Quan, Z.F., Ye, N., Chen, S.J., Cao, S.J., He, M., Yan, Q.G., 2013. High-throughput digital PCR in a low-cost and practical format introduction: the application progress in copy number variation, low-level detection and absolute quantification. Rev. Med. Microbiol. 24 (4), 89–93.
Schmittgen, T.D., Lee, E.J., Jiang, J., Sarkar, A., Yang, L., Elton, T.S., Chen, C., 2008. Real-time PCR quantification of precursor and mature microRNA. Methods 44 (1), 31–38.
Shi, R., Chiang, V.L., 2005. Facile means for quantifying microRNA expression by real-time PCR. Biotechniques 39 (4), 519–525.
Stanley, R.J., 2001. Inherent dangers in radiologic screening. AJR Am. J. Roentgenol. 177 (5), 989–992.
Swensen, S.J., Jett, J.R., Hartman, T.E., Midthun, D.E., Sloan, J.A., Sykes, A.M., Aughenbaugh, G.L., Clemens, M.A., 2003. Lung cancer screening with CT: mayo Clinic experience. Radiology 226 (3), 756–761.
Sykes, P.J., Neoh, S.H., Brisco, M.J., Hughes, E., Condon, J., Morley, A.A., 1992. Quantitation of targets for PCR by use of limiting dilution. Biotechniques 13 (3), 444–449.
Thakur, B.K., Zhang, H., Becker, A., Matei, I., Huang, Y., Costa-Silva, B., Zheng, Y., Hoshino, A., Brazier, H., Xiang, J., Williams, C., Rodriguez-Barrueco, R., Silva, J.M., Zhang, W., Hearn, S., Elemento, O., Paknejad, N., Manova-Todorova, K., Welte, K., Bromberg, J., Peinado, H., Lyden, D., 2014. Double-stranded DNA in exosomes: a novel biomarker in cancer detection. Cell Res. 24 (6), 766–769.
Vogelstein, B., Kinzler, K.W., 1999. Digital PCR. Proc. Natl. Acad. Sci. U. S. A 96 (16), 9236–9241.
Wang, P., Lu, S., Mao, H., Bai, Y., Ma, T., Cheng, Z., Zhang, H., Jin, Q., Zhao, J., Mao, H., 2015. Identification of biomarkers for the detection of early stage lung adenocarcinoma by microarray profiling of long noncoding RNAs. Lung Cancer 88 (2), 147–153.
Wulfkuhle, J.D., Liotta, L.A., Petricoin, E.F., 2003. Proteomic applications for the early detection of cancer. Nat. Rev. Cancer 3 (4), 267–275.
Yanez-Mo, M., Siljander, P.R., Andreu, Z., Zavec, A.B., Borras, F.E., Buzas, E.I., Buzas, K., Casal, E., Cappello, F., Carvalho, J., Colas, E., Cordeiro-da Silva, A., Fais, S., Falcon-Perez, J.M., Ghobrial, I.M., Giebel, B., Gimona, M., Graner, M., Gursel, I., Gursel, M., Heegaard, N.H., Hendrix, A., Kierulf, P., Kokubun, K., Kosanovic, M., Kralj-Iglic, V., Kramer-Albers, E.M., Laitinen, S., Lasser, C., Lener, T., Ligeti, E., Line, A., Lipps, G., Llorente, A., Lotvall, J., Mancek-Keber, M., Marcilla, A., Mittelbrunn, M., Nazarenko, I., Nolte-'t Hoen, E.N., Nyman, T.A., O'Driscoll, L., Olivan, M., Oliveira, C., Pallinger, E., Del Portillo, H.A., Reventos, J., Rigau, M., Rohde, E., Sammar, M., Sanchez-Madrid, F., Santarem, N., Schallmoser, K., Ostenfeld, M.S., Stoorvogel, W., Stukelj, R., Van der Grein, S.G., Vasconcelos, M.H., Wauben, M.H., De Wever, O., 2015. Biological properties of extracellular vesicles and their physiological functions. J. Extracell. Vesicles 4, 27066.
Yung, R.C., 2003. Tissue diagnosis of suspected lung cancer: selecting between bronchoscopy, transthoracic needle aspiration, and resectional biopsy. Respir. Care Clin. N. Am. 9 (1), 51–76.
Zhong, Q., Bhattacharya, S., Kotsopoulos, S., Olson, J., Taly, V., Griffiths, A.D., Link, D.R., Larson, J.W., 2011. Multiplex digital PCR: breaking the one target per color barrier of quantitative PCR. Lab Chip 11 (13), 2167–2174.